In situ STM study of the electrodeposition and anodic dissolution of ultrathin epitaxial Ni films on Au(111)

F. A. Möller, J. Kintrup, A. Lachenwitzer, O. M. Magnussen, and R. J. Behm
Abteilung Oberflächenchemie und Katalyse, Universität Ulm, D-89069 Ulm, Germany
(Received 31 March 1997)

A detailed *in situ* STM study of the electrodeposition and electrochemical dissolution of Ni on reconstructed Au(111) electrode surfaces in various electrolytes is presented, demonstrating the electrochemical formation of well-defined, ultrathin, epitaxial Ni films. Formation of Ni nuclei starts below the Ni^0/Ni^{2+} Nernst potential via place exchange of Ni with Au atoms at the elbows of the herringbone reconstruction, followed by nucleation of Ni islands on top of these substitutional Ni atoms at overvoltages $\eta \geqslant 80$ mV, and by nucleation at step edges of the Au substrate at $\eta \geqslant 100$ mV. At submonolayer coverages islands with two different growth morphologies, compact, triangularly shaped and highly anisotropic, needlelike islands, are observed. Upon further growth these islands coalesce and an almost perfect two-dimensional Ni monolayer is formed. Multilayer growth was studied up to coverages of 5 ML; it exhibits a similar layer-by-layer growth, resulting in very smooth Ni films. In atomic-scale observations a hexagonal Ni lattice with a lattice spacing of 2.5 Å is resolved, similar to the (111) orientation in bulk Ni, and with the same orientation as the Au lattice. The order in the highly defective first Ni layer is considerably improved by second-layer deposition. The significant differences to vapor-deposited Ni on Au(111) indicate a structure-decisive role of coadsorbates in the electrochemical environment. Dissolution of the Ni films at potentials positive of the Nernst potential proceeds via formation of etch pits and step-flow etching. [S0163-1829(97)00843-6]

I. INTRODUCTION

The electrochemical deposition of nickel is an important, well-established technical process for the formation of protective coatings. More recently, new applications have emerged for Ni and Ni alloy electrodeposition that require an improved control of the structure and the morphology of the Ni deposit and of the deposition process. These applications include steps in the production of micromechanical devices, the manufacturing of magnetic recording heads, and the deposition of ultrathin films and of metallic superlattices for magnetic sensors. Furthermore, the electrodeposition of Ni can also be utilized for the formation of thin Ni oxide or hydroxide films with important applications in batteries, electrochromic devices, and catalysts. For a better understanding of the atomic and nanometer-scale structure of electrodeposited Ni on metallic substrates as well as of the deposition process we performed an *in situ* scanning tunneling microscopy (STM) study of the initial stages of Ni growth on Au(111) electrode surfaces. First results of this work have been reported recently.[1,2]

Previous studies of Ni electrodeposition focused on the electrochemical behavior and on the micrometer-scale morphology of the Ni deposit on carbon and various metallic substrates in dependence on the deposition conditions.[3–19] Based on electrochemical measurements a deposition mechanism was proposed, where Ni^{2+} is reduced first by a single-electron reduction step to an adsorbed Ni^+ species followed by one or several steps that lead to the deposition of metallic Ni.[4,5,7] The Ni^+ species was attributed to adsorbed NiOH or a Ni salt complex and was supposed to catalyze the Ni deposition reaction[4,5,7] as well as to form intermediates, which inhibit further deposition.[5,8–10] In addition, inhibition by adsorbed hydrogen was suggested.[9,10,20] Ni deposition on Au electrodes was studied by *in situ* x-ray spectroscopy (XANES) (Ref. 21) and by combined electrochemical and quartz crystal microbalance[11,22] measurements, indicating the deposition of a metallic Ni film from typical plating solutions. A central subject of many studies is the influence of the electrolyte composition, in particular, the role of boric acid, which is an important component in technical, Watts-type plating baths. Conventionally, boric acid is supposed to buffer the pH in the near-surface region and thus prevent the precipitation of Ni hydroxides.[14] However, it was also suggested that boric acid influences the deposition by adsorption on the surface[3,13] or acts as a homogeneous catalyst for Ni deposition via formation of an intermediate Ni complex.[12] STM studies of Ni electrodeposition were up to now restricted to measurements of the distribution of Ni grains on the submicrometer scale.[18,19]

The structure of single crystalline Au(111) surfaces used as substrates in this study has been studied extensively under ultrahigh vacuum (UHV) conditions[23–26] as well as in the electrochemical environment.[27–34] Clean Au(111) crystals in UHV exhibit a surface reconstruction, where the atoms in the Au surface layer are contracted uniaxially by 4.5% along the [110] direction. This causes a small vertical modulation pattern in form of double rows, clearly visible by STM. For well-prepared surfaces domains of two different directions of contraction alternate periodically, resulting in a zigzag (or herringbone) structure of the modulation pattern.[24,25] At the bending points (''elbows'') of the modulation rows the topmost Au layer exhibits two-dimensional dislocations, resulting in a distortion of the Au lattice at these positions.[24,25] The same surface reconstruction is observed on Au(111) samples prepared by annealing in the flame of a Bunsen burner and subsequently immersed into pure (metal-free) acidic or salt

solutions at potentials negative of a critical potential, which is determined by the anion species of the electrolyte.[27–34] In particular, well-annealed samples exhibit the same long-range zigzag pattern found in UHV.[33] Upon increasing the potential above this critical value a reversible surface phase transformation to an unreconstructed (1×1) lattice is observed.[27–34] After decreasing the potential the reconstruction is formed again, albeit with a more random arrangement of the double-row domains. Hence, in the potential range of Ni deposition the Au electrode is always reconstructed. This is beneficial for the comparison with metal growth under UHV conditions, where growth of the admetal always occurs on Au surfaces that exhibit the same reconstruction.

In contrast to electrodeposited films, vapor deposition of ultrathin Ni,[25,35–37] Co,[38,39] and Fe (Refs. 35, 40) films on reconstructed Au(111) surfaces was studied in detail in previous UHV-STM experiments. These experiments revealed that all three metals nucleate preferentially at the elbow sites of the herringbone reconstruction, resulting in the formation of regular arrays of admetal islands. Based on UHV-STM observations at very low coverages and on thermodynamic considerations, this phenomenon was recently attributed to a two-step mechanism, involving place exchange at the elbow sites and subsequent nucleation *on top* of these substitutional Ni atoms.[37] Second-layer islands nucleate on the hexagonally shaped Ni monolayer islands at coverages as low as 0.3 ML.[35,36] Although the atomic lattice of the Ni islands was not resolved, a pseudomorphic structure was proposed for monolayer islands, whereas for bilayer and thicker films the STM observations seem to indicate a nonpseudomorphic arrangement.[25,36]

We have recently performed an extensive *in situ* STM study of the initial stages of Ni electrodeposition on various Au and Cu single-crystal surfaces.[1,2,41–43] Here we present STM observations of Ni deposition on Au(111), which provide detailed, atomic-scale information on the nucleation behavior, the growth from submonolayer coverages up to multilayer films, and the dissolution of ultrathin Ni films. This work focuses on the atomic and defect structure of the Ni deposit, the resulting morphology of the Ni films, the interaction with the Au herringbone reconstruction, and the mechanisms of Ni growth and dissolution. In particular, a layer-by-layer growth is revealed for Ni on Au(111), resulting in the formation of atomically smooth, (111)-oriented multilayer films of metallic Ni. The role of structural defects in the nucleation, growth, and dissolution of these Ni films as well as the removal of such defects with increasing film thickness, induced by an increased tendency to form a well-ordered Ni lattice, is highlighted. Selected aspects concerning the initial stages of Ni nucleation and growth[1] and the formation of highly anisotropic Ni submonolayer islands[2] have been published separately and will be only briefly reviewed for the sake of a complete and comprehensive presentation. In addition, observations on the kinetically hindered anodic dissolution of the Ni film indicate passivation of the topmost Ni layer by an adsorbed surface species.

II. EXPERIMENT

Two different types of home-built scanning tunneling microscopes for *in situ* electrochemical experiments were used in the experiments. The first was described in detail in Ref. 44, the second one is based on a design by Besocke.[45] Tunneling tips were prepared by electrochemical etching of a polycrystalline tungsten wire and manually coated with Apiezon wax leaving only the last 10 μm of the tip exposed. Tip and sample potential were independently kept under potentiostatic control and measured versus a Ag/AgCl (KCl saturated) reference electrode, with the tip potential usually kept 50–100 mV negative of the sample potential. The Au(111) sample was oriented and cut to $\pm0.3°$, mechanically polished with diamond paste down to 1 μm grain size, and finally electropolished in cyanide solution. Prior to each experiment the Au crystal was annealed in a propane flame as described in Ref. 27, slowly cooled down in air, and then transferred into the electrochemical cell of the STM. Subsequently, the sample was immersed under potential control at a potential of -0.2 V. As can be seen in the STM images this procedure results in a well-ordered Au surface with large atomically flat terraces, which exhibit the herringbone reconstruction at all potentials down to the onset of Ni deposition. Electrolytes were 10^{-3} M $NiSO_4$, modified Watts electrolyte (10^{-2} M H_3BO_3, 10^{-3} M $NiSO_4$, 10^{-4} M HCl), and 10^{-3} M $Ni(NO_3)_2$, prepared from pro analysis grade $NiSO_4$ and $Ni(NO_3)_2$ (Merck), suprapure H_3BO_3 and HCl (Merck), and Milli-*Q* water. STM images were obtained in constant current mode with tunneling currents typically between 1 and 10 nA and are presented as topview images with darker colors corresponding to lower surface areas. At the negative potentials required for Ni deposition noticeable hydrogen evolution occurs at the Au sample (see below). This causes major experimental problems in the STM measurements due to decreased tip stability, which may either result directly from gas bubble formation or by precipitation of Ni hydroxide species, caused by the corresponding change in surface pH. It is noteworthy that these problems were less pronounced in the Watts electrolyte, where the presence of boric acid is thought to buffer the surface pH and to form a surface-active complex, which lowers the Ni overpotential and partly inhibits hydrogen evolution.[12]

III. RESULTS

A. Cyclic voltammetry

Prior to the STM measurements the electrodeposition of Ni on Au(111) was characterized by cyclic current-voltage curves (cyclic voltammograms), which were recorded in a separate electrochemical cell using the dipping technique. A typical voltammogram obtained in the Watts electrolyte is shown in Fig. 1. The predominant feature in the cathodic potential sweep is a large negative current caused by the hydrogen evolution reaction. The onset of Ni deposition is only barely discernible as a broad shoulder at about -0.6 V on top of this current. No negative current peak is observed at potentials positive of the Ni^0/Ni^{2+} Nernst potential (-0.52 V at 10^{-3} M Ni^{2+}, see arrow in Fig. 1) indicating the absence of an underpotential deposition effect for Ni on Au(111). Upon reversing the potential scan an increasing positive current, which indicates the onset of Ni dissolution, is observed at potentials positive of the Ni^0/Ni^{2+} Nernst potential (-0.52 V at 10^{-3} M Ni^{2+}) giving rise to a single stripping peak at ≈200 mV higher potentials (the peak posi-

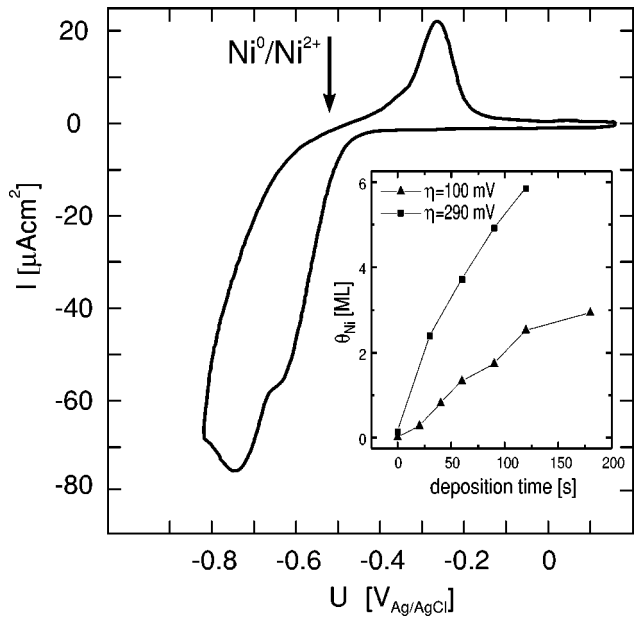

FIG. 1. Cyclic voltammogram of Au(111) in Watts electrolyte (the arrow indicates the Ni^0/Ni^{2+} Nernst potential). The inset shows the Ni coverage θ_{Ni}, derived from the charge of the Ni dissolution peak, as a function of the deposition time for two overpotentials η.

tion depends on the scan rate and the amount of deposited Ni and ranges between -0.4 and -0.2 V). The large shift of the peak to anodic values indicates that Ni dissolution is kinetically hindered. In subsequent potential cycles the voltammogram is completely reproducible, suggesting that the Au(111) surface is not altered significantly by deposition and stripping of Ni.

The amount of deposited Ni was assessed by keeping the potential at a fixed deposition potential for a period between 20 s and 15 min and then measuring the charge in the Ni dissolution peak, which is well above the hydrogen evolution range. According to these coulometric measurements, noticeable Ni deposition starts at about -0.6 V, i.e., at overpotentials $\eta \geqslant 80$ mV. Assuming that the entire anodic charge can be attributed to the Ni dissolution reaction $Ni^0 \rightarrow Ni^{2+} + 2e^-$ and that the Ni is deposited as a metallic, (111)-oriented Ni film (see below), i.e., that each Ni layer contains $(d_{Ni}^2\sqrt{3}/2)^{-1} = [(2.5\ \text{Å})^2\sqrt{3}/2)^{-1} = 1.84 \times 10^{15}$ atoms/cm^2 corresponding to a charge of 590 μC/cm^2, the nominal Ni layer thickness can be estimated. As shown in the inset in Fig. 1 this thickness increases continuously but not linearly with time for a fixed deposition potential. Instead the growth rate apparently decreases with increasing coverage, which was also observed in the STM experiments (see below).

Very similar voltammograms were observed in pure $NiSO_4$ and $Ni(NO_3)_2$ solution. Here the overpotentials required for measurable Ni deposition were $\geqslant 100$ mV $[Ni(NO_3)_2]$ or $\geqslant 120$ mV $(NiSO_4)$, i.e., only slightly higher than in the borate-buffered Watts solution. The results are in agreement with previous electrochemical and quartz-crystal microbalance studies on polycrystalline Au in Watts electrolytes with considerably higher Ni^{2+} concentrations.[11,22] In addition, it was shown in these studies that the charge in the Ni stripping peak can be attributed solely to the oxidation of metallic Ni to Ni^{2+},[22] thus justifying the above procedure of measuring the Ni coverage.

B. Nucleation

As described in detail in Ref. 1 the nucleation of Ni on the reconstructed Au(111) surface strongly depends on the applied overpotential η. The nucleation and growth at $\eta = 80$ mV, the minimal overpotential required for Ni deposition *on top* of the Au surface, is illustrated in Fig. 2. In this experiment a large terrace on the surface of a freshly annealed sample was initially observed at -0.2 V, where only the characteristic zigzag pattern of double rows of the herringbone reconstruction was visible, and then the potential was changed to -0.6 V. Directly after the potential step [Fig. 2(a)] no Ni islands are found on the surface. However, a distinct change is observed at the bending points (elbows) of the dislocation rows, where the two-dimensional lattice of the Au surface layer is distorted.[25] These elbows are now decorated by small ''holes'' of about 20 Å in width and 0.5 Å in apparent depth. The ''holes'' are observed in the STM images for potentials more negative than the Ni^0/Ni^{2+} Nernst potential and can be attributed to substitutional Ni atoms, which have replaced Au atoms of the distorted surface lattice

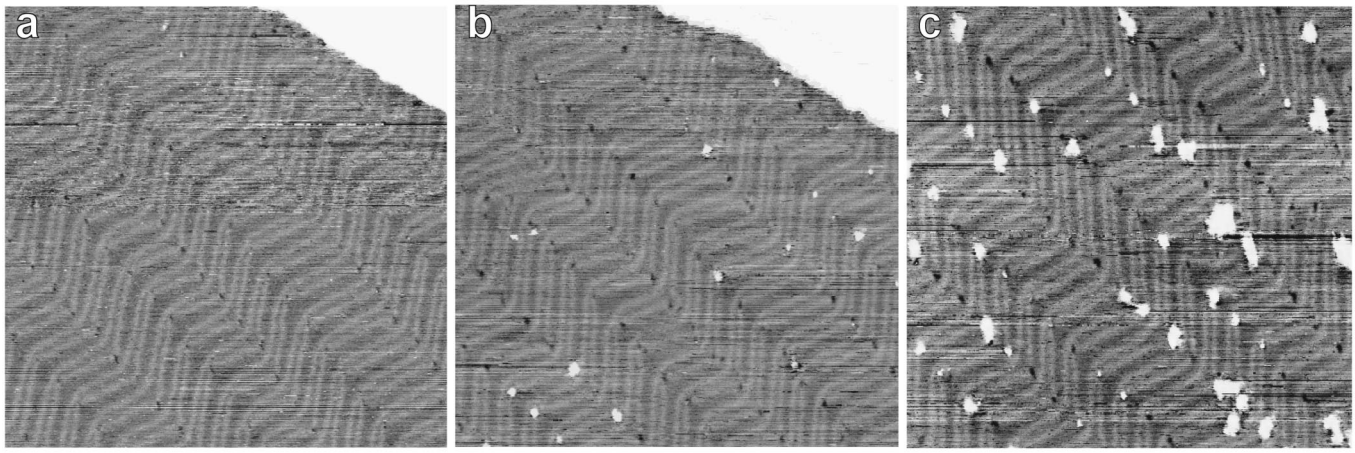

FIG. 2. Series of STM images of Au(111) in Watts electrolyte recorded (a) directly after a potential change from -0.2 to -0.6 V, (b) after 3 min at -0.6 V, and (c) after 20 min at -0.6 V showing slow nucleation and growth of Ni adlayer islands at the elbows of the herringbone reconstruction (1050×1050 Å^2).

at the elbow sites.[1] The depth of the holes is approximately equal to the difference of Au steps and Ni monolayer islands (see Sec. III C) and can only partly be accounted for by the smaller size of the Ni atoms (≈ 0.3 Å depth according to a hard-sphere model), indicating contributions from electronic effects.

In Fig. 2(b), recorded 3 min later at -0.6 V, nucleation of the first Ni islands *on top* of the Au surface can be seen. At this potential Ni islands nucleate exclusively at the elbows, where the Au surface atoms have been substituted by Ni. With time, number, and size of these nuclei slowly increase as illustrated in Fig. 2(c), where 50% of the elbows are decorated by Ni adislands after a deposition time of 20 min. Even after deposition times of 1 h no nucleation at the Au step edges was observed at -0.6 V. This indicates that the elbows are the preferred nucleation sites at this potential and that subsequent growth is restricted to Ni adatom attachment at Ni island edges, while Au step edges are inert under these conditions. A very similar nucleation behavior was observed for the deposition of Ni on reconstructed Au(111) in UHV,[25,37] where it was also attributed to a two-step mechanism, consisting of place exchange of Ni with Au surface atoms, followed by adisland nucleation *on top* of substitutional Ni.

At only 20 mV higher overpotentials the nucleation behavior changes distinctly. This is shown in the STM images in Figs. 3(a) and 3(b), recorded in the vicinity of a Au step before and after a potential step to -0.63 V. At this potential Ni monolayer islands are rapidly formed at the lower terrace side of the Au steps, from where they grow onto the terraces until the entire surface is covered by a Ni monolayer. Only a few isolated islands are formed in the center of the terraces at this potential, indicating that the rate of nucleation at elbows is not significantly higher than at $\eta = 80$ mV. Hence nucleation at step edges becomes the dominant mechanism at $\eta \geqslant 100$ mV.

C. Submonolayer growth

The formation of a Ni monolayer on the reconstructed Au(111) surface can be seen in the series of successively recorded STM images presented in Fig. 4. This series was recorded in Ni nitrate solution; very similar results (apart from small differences in the potential) were obtained in Ni sulfate and in Watts solution (compare, e.g., Ref. 2). In Fig. 4(a) a single Au terrace is shown at a potential of -0.6 V, where only the corrugation pattern of the herringbone reconstruction is visible. At the beginning of the following image [upper edge of Fig. 4(b)] the potential was lowered to -0.63 V, resulting in the formation of Ni monolayer islands at the lower edge of the image. In the two subsequent images [Figs. 4(c) and 4(d)], recorded at -0.62 V to decrease the rate of Ni growth, these islands spread until the Au surface is almost completely covered. It should be noted that the Ni islands continuously grow during the recording of the images and that the images consequently do not show a static surface topography. Ni islands with two different kinds of growth morphologies are discernible in the images: compact, often triangularly shaped islands and metastable, strongly anisotropic, needlelike islands.

The compact islands exhibit a pronounced, long-range, hexagonally ordered modulation pattern (''white dots'') with

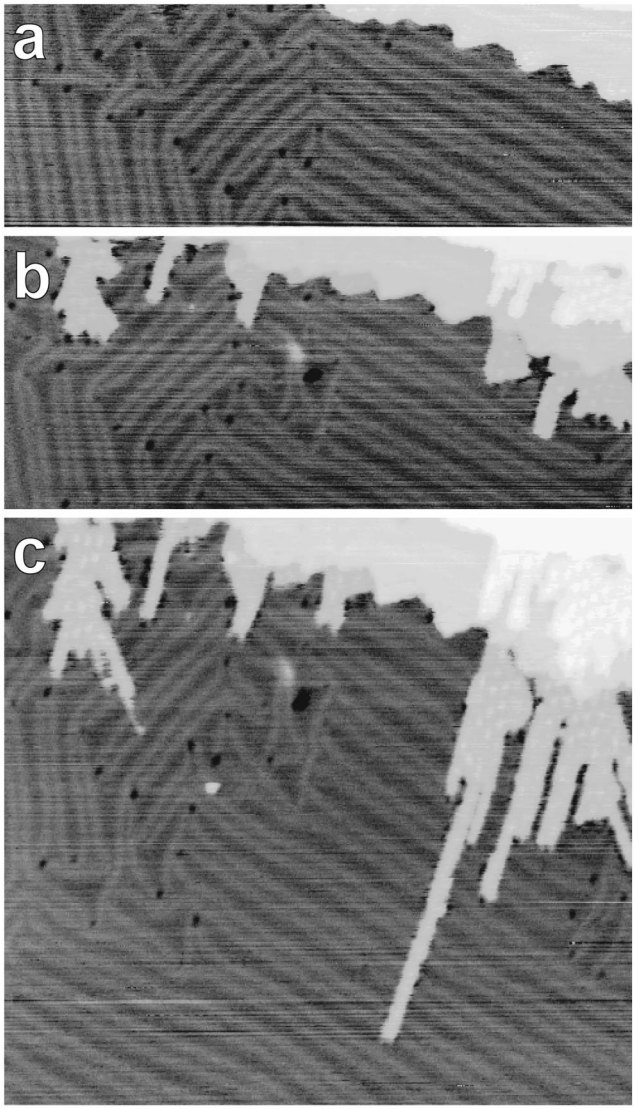

FIG. 3. Series of STM images recorded on Au(111) in Watts electrolyte (a) at -0.59 V (1150×450 Å^2), (b) after 3 min at -0.63 V (1150×550 Å^2), and (c) successively at -0.6 V (1150×760 Å^2), showing nucleation of Ni islands at the Au steps and growth of anisotropic Ni needle islands.

a nearest-neighbor spacing of ≈ 22 Å and a typical amplitude of 0.6 Å. The origin of this modulation is the mismatch between adlattice and substrate lattice (moiré pattern) as shown by atomic-resolution STM observations (Fig. 5). In Fig. 5(a) the nearly hexagonal atomic lattice of the reconstructed Au(111) surface with a lattice spacing of 2.9 Å can be seen. In Fig. 5(b) the same surface area after deposition of a Ni monolayer is shown. Here the characteristic long-range modulation is superimposed by a smaller hexagonal lattice with a lattice spacing of 2.5 Å, which is parallel oriented with respect to the Au lattice. This lattice spacing is almost identical to that in the (111) plane of metallic Ni (2.49 Å). From the lattice parameters ($d_{\mathrm{Ni}} = 2.49$ Å and $d_{\mathrm{Au}} = 2.885$ Å) the lattice spacing of the long-range modulation can now be calculated as $d_{\mathrm{moiré}} = 21.2$ Å, in good agreement with the experiment. Also the modulation amplitude of 0.6 Å is close to that calculated from a hard-sphere model. The steps at the edges of the compact islands consist of straight

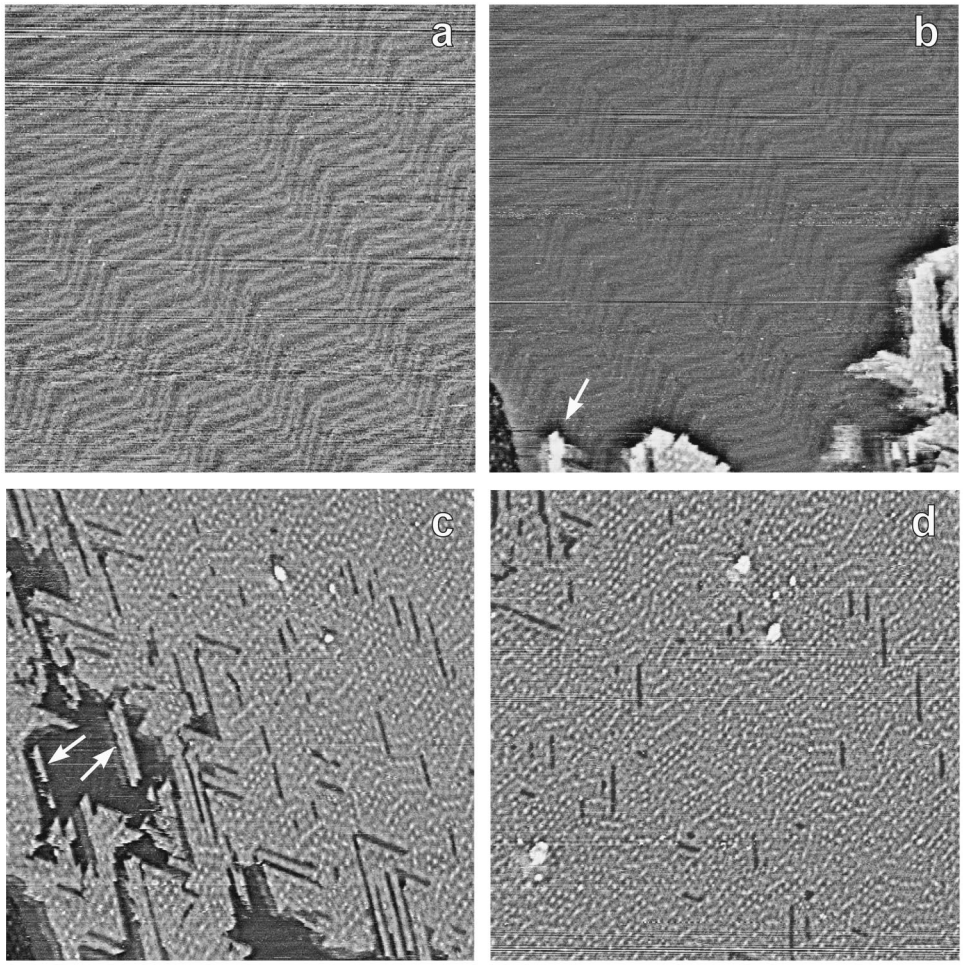

FIG. 4. Series of STM images of Au(111) in Ni nitrate solution recorded successively in intervals of 3 min (a) at -0.6 V, (b) at -0.63 V, and (c,d) at -0.62 V, showing the growth of a complete Ni monolayer (1400×1400 Å^2). The slow scan direction, which corresponds to the time axis, is from bottom to top in the images in (a,c) and from top to bottom in those in (b,d).

sections, which run along the close-packed directions of the Ni lattice. The average island height is 1.7 Å with respect to the Au surface. Although the Au reconstruction is observed on the neighboring (Ni-free) Au substrate it is currently not clear whether the reconstruction is maintained beneath the compact Ni monolayer islands or whether the topmost Au layer is transformed into an unreconstructed (1×1) lattice during the growth of these islands.

Examples of the much more unusual, needlelike islands can be observed in Fig. 3(c), as well as in Figs. 4(b) and 4(c) (see arrows). Structure and growth of these islands have been described in detail in a previous publication.[2] The most important results are the following: (a) The needle islands are always oriented perpendicular to the double rows of the reconstruction, i.e., they run along the $[1\bar{1}0]$ direction, where the topmost Au layer is contracted by 4.5%: (b) The islands have certain preferred widths, which are $n(11.5\pm1.0\,\text{Å})$ with $n\leqslant4$. (c) Needles grow predominantly in the longitudinal direction, but can also grow in width. However, needles wider than ≈50 Å transform into islands of the compact type. (d) The height of the needles is only 1.3 Å and they do not exhibit the moiré pattern of the compact islands. Instead, the double rows of the neighboring reconstructed Au surface are continued on top of these islands, indicating that the reconstruction of the underlying Au substrate is not lifted. A structural model of the needle islands that explains this growth behavior has been given in Ref. 2 and will be briefly reviewed in Sec. IV A.

This complex, potential-dependent nucleation and growth behavior also strongly influences the structure of the completed Ni monolayer. As seen in Fig. 4(c) a large number of individual needle and compact islands are formed on the Au surface, most likely due to nucleation at elbow sites. Often needle islands nucleate at the elbows, resulting in parallel running, neighboring needles at well-defined distances. At coverages close to a full monolayer [Fig. 4(d)] this results in needlelike troughs between former needles. These troughs are filled only slowly and predominantly by deposition at the trough tips, i.e., in a similar way as the needles. The moiré pattern of the completed Ni monolayer is highly defective [Fig. 4(d)] and a true hexagonal arrangement is found only in small local patches. Instead, strong distortions and defects can be observed, indicating a distorted Ni adlattice. This can be explained by the formation of multiple-domain boundaries during the growth of the Ni layer and will be discussed in detail in Sec. IV C.

D. Multilayer growth

As visible in Fig. 4(d), nucleation of second-layer Ni islands starts only after the first layer is almost completed.

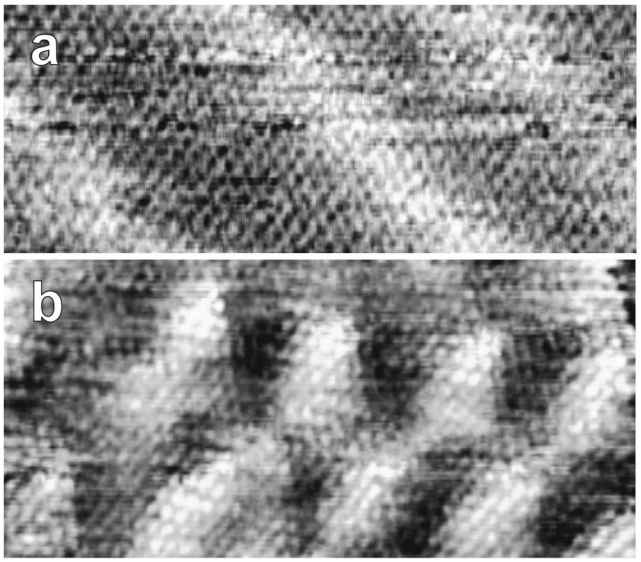

FIG. 5. Atomic-resolution STM images recorded subsequently on Au(111) in Ni sulfate solution showing (a) the bare reconstructed Au(111) surface at -0.06 V (100×40 Å^2) and (b) the atomic lattice of the Ni monolayer at -0.61 V (100×50 Å^2).

Other series of images (not shown) seem to indicate that these second-layer islands are often formed at the former elbow sites. Since the nucleation sites on top of the Ni adlayer can often not be correlated with the underlying substrate structure, a more quantitative analysis is not possible. Nevertheless, second-layer nucleation at or close to the elbow sites appears likely for two reasons: First, the local distortions in the Au substrate at these sites most likely also influence the structure of the first *on top* Ni layer and, second, the first layer in the vicinity of these sites may be distorted by domain boundaries, due to the peculiar nucleation and growth behavior of the Ni monolayer (see Sec. IV C).

The further growth of the Ni film is shown in the series of STM images in Fig. 6, recorded at -0.66 V in the Ni sulfate solution (i.e., only 20 mV below the potential where Ni deposition is observed in 10^{-3} M $NiSO_4$). Again, very similar results were obtained in the Ni nitrate and in the Watts solution. Figure 6(a) shows two Au terraces, separated by a monoatomic Au step (running from the left edge to the upper right corner of the images), which are almost completely covered by a monolayer of Ni. As in Fig. 4(d) the ''dots'' of a rather disordered moiré pattern are clearly visible. In addition, a number of second-layer islands are found along the Au step as well as on the terraces. In the image in Fig. 6(b), recorded 20 min later, the surface is covered by approxi-

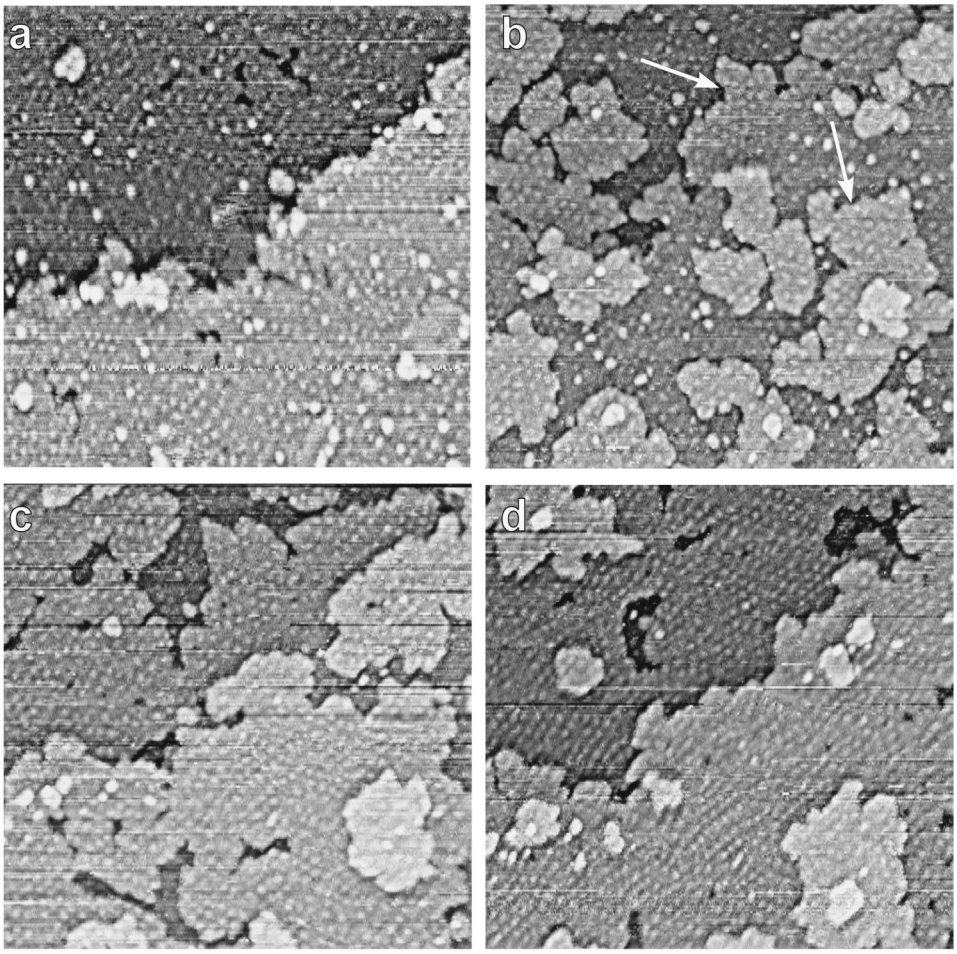

FIG. 6. Series of STM images of Au(111) in Ni sulfate solution showing the growth of the Ni deposit at -0.66 V (900×1000 Å^2). The images are recorded at (a) 55 min, (b) 75 min, (c) 100 min, and (d) 120 min after the potential was changed into the potential range of Ni deposition and corresponding to average Ni coverages of (a) 1 ML, (b) 1.5 ML, (c) 2 ML, and (d) 2.3 ML.

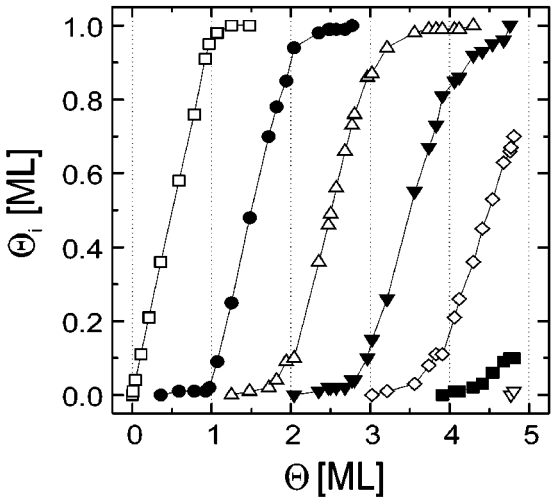

FIG. 7. Plot of the occupation θ_i of Ni layer 1 (□), 2 (●), 3 (△), 4 (▼), 5 (◇), 6 (■), and 7 (▽) as a function of total Ni coverage θ, showing the almost perfect layer-by-layer growth on Au(111). The data was obtained by quantitative evaluation of series of STM images recorded in Watts electrolyte.

mately 1.5 ML of Ni. The second Ni layer has now grown 100 to 200 Å from the Au step edge and on the smooth, Ni-monolayer-covered terrace second-layer islands with diameters up to 300 Å have formed at the positions of the initial nuclei. Also a few small third-layer islands can be observed on the larger second-layer islands. The second- and higher-layer islands usually do not exhibit the straight steps along the main lattice directions favored for the monolayer islands and needlelike islands are completely absent. Instead, more isotropic, round-shaped islands with steps consisting of small sections, which locally follow the main lattice directions, are typically observed. During the growth process neighboring islands merge to larger islands of a more irregular shape, with the shape of the original islands almost unchanged. This indicates a low mobility of Ni atoms along the island edges (see also Sec. IV C). After another 25 min [Fig. 6(c)], at an average coverage of 2 ML, 90% of the second layer is completed while less than 10% of the surface is covered by islands of layer 3. The step of the underlying Au substrate is clearly recognizable, illustrating the high uniformity of the deposit. The last image [Fig. 6(d)], recorded again 20 min later and corresponding to 2.3 ML Ni, shows an almost completed second layer, several third-layer islands, and a small fourth-layer island on top of each of the two largest third-layer islands. About 2/3 of the third layer islands in Fig. 6(d) are formed along the position of the underlying Au step edge, indicating that new adislands form predominantly by heterogeneous nucleation at defect sites. For third- and higher-layer adislands such a nonuniform distribution was typically observed, whereas for the second layer the density of nuclei was generally higher and the islands were more uniformly distributed on the surface. This is probably related to the high defect density in the first Ni layer (see Secs. III C and IV D).

A similar layer-by-layer growth was observed also for the growth of the following layers up to a coverage of (at least) 5 ML for low deposition rates ($80 \leqslant \eta \leqslant 200$ mV). This is illustrated in the plot in Fig. 7. Here the occupation of the

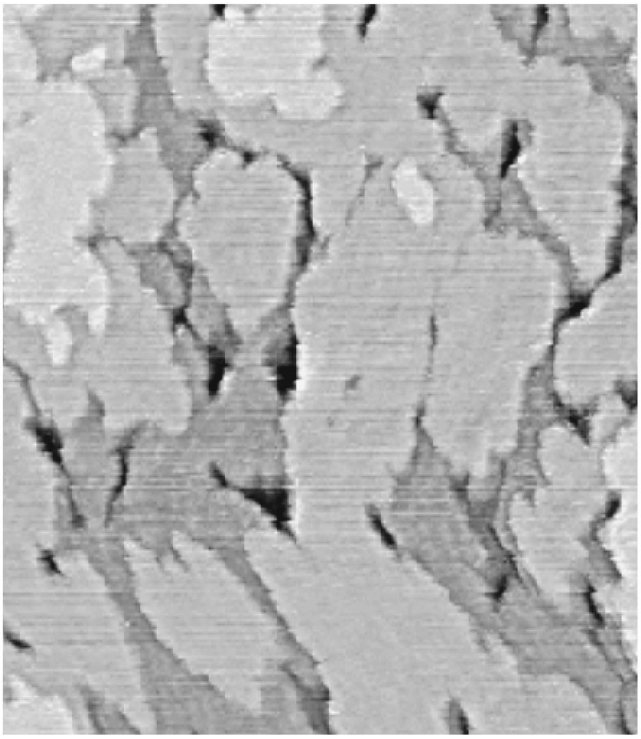

FIG. 8. STM image of a 4.8 ML thick Ni film on Au(111) at -0.72 V in Watts electrolyte (800×930 Å^2).

individual Ni layers θ_i in a series of STM images, recorded during deposition in the Watts electrolyte, was evaluated quantitatively and plotted versus the total coverage θ. An STM image of a 4.8 ML Ni film, the maximum thickness investigated, is shown in Fig. 8. More than 90% of the surface is covered by a film of 4 or 5 ML thickness and only a few isolated deeper holes or islands of layer 6 are visible. The characteristic moiré pattern with the same, layer-independent nearest-neighbor distance between the dots is discernible on the Ni islands up to the 6th layer, although its amplitude decreases with thickness. Hence the multilayer films have the same atomic structure as the monolayer. The height of the second layer islands is 1.9 Å, that of the islands of all following layers 2.0 Å, i.e., within the experimental precision identical to the layer spacing of (111)-oriented metallic Ni (2.03 Å). Thus, the much lower average height of the monolayer islands (1.7 Å) is probably caused by electronic contributions in the STM images. In addition, a similar surface topography of the Ni films was also observed in experiments, where the STM tip was removed from the solution during deposition to rigorously exclude tip shielding effects. These observations demonstrate that smooth Ni films of well-defined structure and thickness can be formed under these conditions.

The absolute rate of Ni deposition obtained from the series of STM images is a factor 2–5 lower than that estimated from the electrochemical experiments described in Sec. III A. Since experiments where tip position or scan range were changed revealed no differences in film morphology or thickness, the different rate cannot be caused by tip shielding effects. Nevertheless, this effect is probably related to an experimental artifact, e.g., the very different geometry of the electrochemical cell in the STM and in the voltammetric

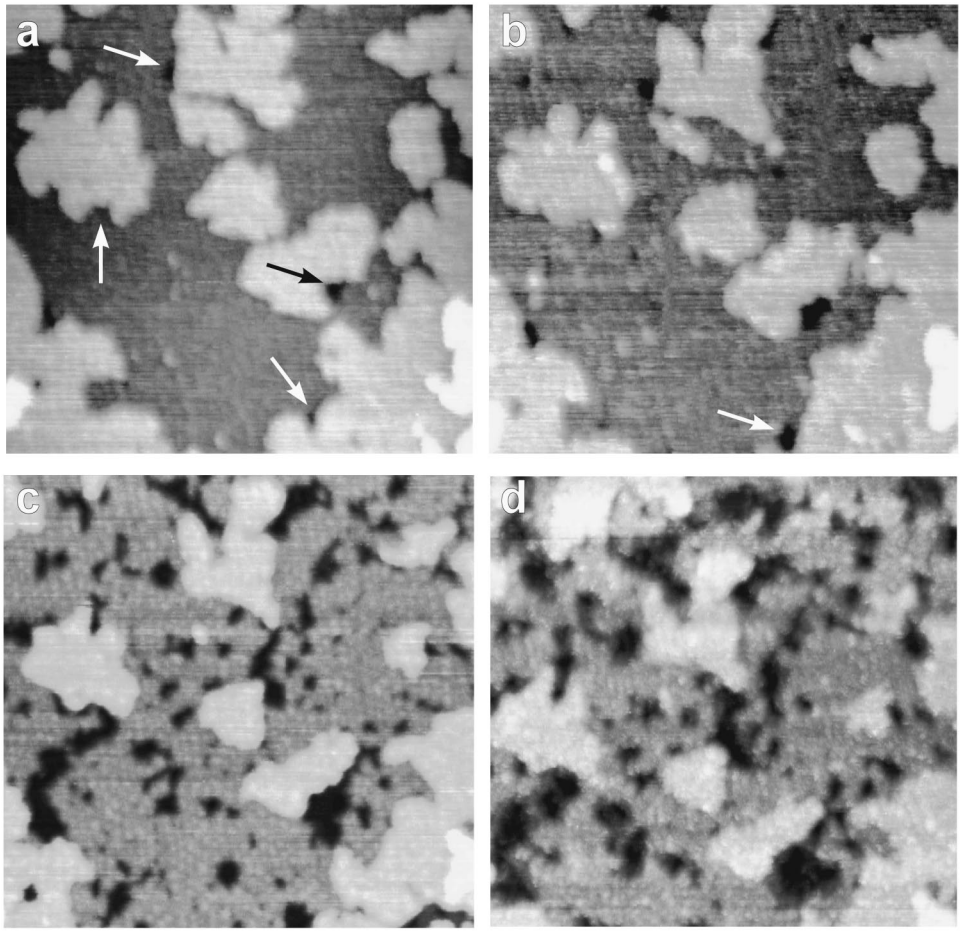

FIG. 9. Series of STM images showing the dissolution of the Ni film on Au(111) in Ni sulfate solution (a) at −0.46 V, (b) 7 min later at −0.36 V, (c) 15 min after (a) at −0.36 V, and (d) 40 min after (a) at −0.16 V (900×1000 Å^2).

measurements. In addition, a decrease in the deposition rate with increasing deposition time (at constant overpotential) was found in the STM observations. Since this was also observed in the electrochemical measurements, this must be related to a growth-inhibiting phenomenon, such as passivating adsorbates.

Finally, it is worth mentioning that the defect structure of the Ni film changes with growing film thickness. This is indicated by distinct changes in the moiré pattern on the second- and higher-layer terraces in Fig. 6. Obviously, the dots of the moiré pattern on the second-layer islands in Fig. 6(b) (some indicated by arrows) are arranged in much larger hexagonally ordered domains than those on the Ni monolayer. After completion of the second layer [Figs. 6(c) and 6(d)] the entire surface exhibits this improved hexagonal order, with individual hexagonal domains of up to several hundred Å in diameter. These changes cannot be attributed to a better ordered second layer on top of a disordered first layer, since the moiré pattern reflects the lattice mismatch at the Au(111)-Ni interface (mismatch between different Ni layers could also give rise to a moiré pattern, but with a drastically different nearest-neighbor spacing). Instead, it has to be related to an increase in order in both layers, i.e., to a rearrangement of the underlying first layer during second-layer deposition. The improved order in the moiré pattern in turn indicates an improvement in the atomic lattice and the removal of lattice defects, such as domain boundaries. Deposition of further layers causes only small changes in the order established after second layer deposition. A detailed discussion of this ordering process is given in Sec. IV C.

E. Dissolution

In this section preliminary results on the anodic dissolution of the ultrathin Ni films on Au(111) in Ni sulfate solution (pH 4) are presented. This process is illustrated in Fig. 9 by a series of images showing the dissolution of a 2.5 ML Ni film at increasingly positive potentials. The dissolution starts at −0.46 V [Fig. 9(a)] by the formation of small holes (see arrows). At this potential the holes are formed exclusively at the lower edge of the third-layer Ni islands. Subsequently, the potential was slowly changed over a period of 7 min to −0.36 V, where Fig. 9(b) was recorded. By comparing Figs. 9(a) and 9(b) an increase in the size of the holes and a slow, uniform etching along the steps of the third-layer islands can be observed. As can be seen in Fig. 9(c), recorded 22 min later at the same potential, holes are formed now also within the atomically flat terraces of the Ni film. Most of these holes are two or three Ni layers deep, i.e., they extend down to the Au substrate, although a precise measurement is difficult for the smaller holes due to the finite size of the tip. At even higher potentials dissolution proceeds via the same etch pit formation and step-flow processes [see Fig. 9(d)] causing slow disintegration of the Ni film. In all of the images in Fig.

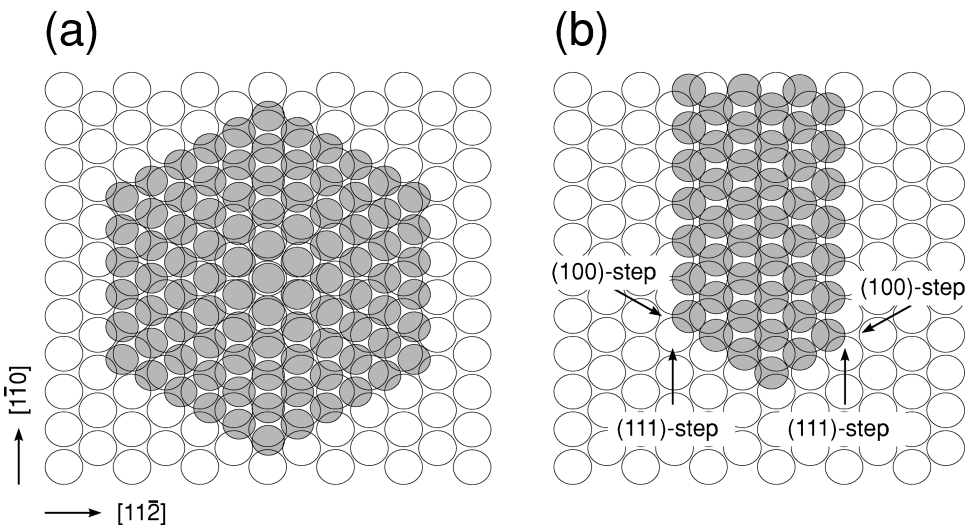

FIG. 10. Models showing the proposed atomic structure of the Ni deposit (a) of compact monolayer islands and multilayer films (b) of the anisotropic needlelike islands. For simplicity, the slight distortions of the Au lattice caused by the reconstruction have been omitted.

9 the moiré pattern is faintly discernible [particularly well in Fig. 9(c)]. This demonstrates that the structure of the Ni deposit is not changed in this potential range. The dissolution process continues until only single Ni monolayer and multilayer islands, corresponding to areas between former holes, remain on the surface, which in the further course of the experiment are also dissolved. Usually, the Ni film was completely dissolved at potentials $\geqslant -0.1$ V. No morphological changes of the Au substrate, such as changes in the shape of the Au steps, monoatomic pits, or Au islands on the terraces, were observed after a Ni deposition/dissolution cycle. This suggests that place exchange of Ni with Au surface atoms is restricted to the elbow sites and does not occur (or occurs only at negligible rate) at undistorted Au surface lattice sites. According to these observations, the dissolution behavior is distinctly different from the layer-by-layer growth behavior found for Ni deposition. Possible explanations for these differences will be given in Sec. IV D.

IV. DISCUSSION

A. Structure of the Ni deposit

In this section the atomic structure of the deposited Ni monolayer and multilayer islands is discussed, related to previous electrochemical data, and compared with the structure of vapor-deposited Ni. The predominant structure, which was observed for larger Ni monolayer islands and all coverages $\geqslant 1$ ML, is a hexagonal lattice with nearest-neighbor distances as in bulk fcc Ni and with an orientation parallel to the Au substrate lattice [Fig. 10(a)]. Due to the different lattice constants of Ni and Au the adatoms occupy not only the energetically preferred hollow sites of the Au lattice, but also the less favorable bridge and top sites, as illustrated directly by the observed moiré pattern. This indicates that even in monolayer-thick Ni films the lateral interactions within the Ni lattice dominate the Ni lattice structure and that the major effect of the underlying Au lattice apparently is to fix the adlattice orientation. In contrast, for vapor-deposited Ni monolayer islands on Au(111) in UHV no moiré pattern was found, indicating pseudomorphic growth of this layer.[25,35,36] Hence, in this latter case the substrate corrugation exerts a structure-decisive influence on the adlayer. This structural difference could be explained either by an increased interaction between the Ni adatoms or by a decrease in the Ni-Au corrugation potential (i.e., the variation of the Ni-Au interaction between different adsorption sites) in the electrochemical environment. Both effects could be caused by an adsorbate on top of the electrodeposited Ni layer (possible adsorbate species will be discussed in Sec. IV E) or by the electric field of the electrochemical double layer. However, in view of the very negative potential of zero charge reported for (polycrystalline) Ni,[46] which is close to the used deposition potentials, a major effect of the latter field-induced changes seems unlikely.

The absence of a moiré pattern and the different island height of the metastable, needlelike Ni monolayer islands suggest that the structure differs from the predominant Ni(111)-like lattice as well as from the structure of vapor-deposited Ni islands, where these needlelike islands were never observed. To explain these observations as well as the unusual shape of these islands a model assuming an uniaxially incommensurate Ni adlattice was proposed [Fig. 10(b)].[2] According to this model, the Ni atoms are pseudomorphically arranged along the needle direction, but contracted perpendicular to that direction up to a Ni nearest-neighbor spacing of 2.5 Å. Due to this, close-packed, (111)-type steps are formed along the sides of the needle, whereas at the needle tip the steps are of the more open (100) type. During island growth Ni adatoms have a high mobility along the (111)-type steps and hence are transported to the needle tip, where they are trapped in the more strongly binding (100)-type step sites, resulting in the observed anisotropic growth. The orientation of the needle islands was attributed to the weak anisotropy of the underlying reconstructed Au surface layer (see below).[2] The existence of a metastable Ni monolayer phase that is partly in registry with the substrate suggests that the presence of the electrolyte only leads to a slight dominance of the lateral Ni-Ni interactions over the Ni-Au corrugation potential. This could explain why small islands, stabilized by size and/or kinetic effects, can have a structure that is closer to the pseudomorphic arrangement found in UHV.

B. Ni interaction with the Au(111) reconstruction

The deposition potential of Ni is much more negative than that of the metals typically employed for *in situ* structural

studies of monolayer and multilayer deposition, such as Cu, Ag, Pb, or Tl. Consequently, Ni is deposited not on the simple hexagonal lattice of the unreconstructed surface, which prevails in the positive potential range, but on the more complex, reconstructed surface. As shown above, this has significant influence on the nucleation and submonolayer growth of Ni: First, by the small local lattice anisotropy caused by the uniaxial contraction of the surface layer, which may affect admetal surface diffusion and growth, and second, by the long-range, periodic surface heterogeneity, which may provide a variety of energetically different, locally separated surface sites for admetal nucleation and growth.

The influence of the Au reconstruction on the nucleation behavior of Ni has been illustrated in Sec. III B and is discussed in detail in Ref. 1. The preferred nucleation at the elbow sites was explained by an initial nucleation via place exchange at the elbow sites and subsequent growth *on top* of the substitutional Ni atoms. This mechanism governs the Ni electrodeposition at low overpotentials[1] as well as the deposition in UHV.[37] Deposition via place exchange requires that the substitutional Ni atoms are thermodynamically stable and that the kinetic barrier for the exchange process is low. Apparently one or both of these conditions are fulfilled only at the elbows, but not at the undistorted hexagonal close-packed lattice sites in between, where no indication for place exchange was found. Interestingly, place exchange was also observed in a UHV-STM study of Ni deposition on the more open Au(110) surface,[47] verifying the general tendency of Ni to substitute Au surface atoms.

Also the growth of the needle islands is influenced by the reconstruction. As shown in Sec. III C the needle orientation is always parallel to the direction, along which the Au surface layer is contracted. Since the reconstruction of the underlying Au substrate apparently is maintained in the presence of the needle islands (see Ref. 2 for details) the slight anisotropy of the reconstructed Au surface layer can directly affect the structure of the Ni adlattice. Assuming the model in Fig. 10(b) is valid, the orientation along the direction of contraction allows a slightly more compact and less anisotropic Ni lattice in these islands than for the other two close-packed directions and should thus be favored.

The combined effects of preferential nucleation at elbows and oriented needle growth may result in nanometer-scale ordering of the Ni deposit on well-prepared herringbone-reconstructed Au surfaces. Here the reconstruction domains are arranged in a periodic zigzag pattern and consequently also the Ni nuclei form a regular pattern. In addition, each elbow is surrounded by two reconstruction domains, which have the same orientation for all elbows along a row. As a result arrays of parallel needles with similar length and alternating orientation in perpendicular direction are often formed (see, e.g., Fig. 4(c) or Fig. 4 in Ref. 2). Hence, the mesoscopic order of the herringbone reconstruction may be employed as a template for the generation of periodic Ni admetal structures on the nanometer scale.[25]

C. Morphology and defect structure of the Ni deposit

The morphology of the Ni islands in the first layer differs significantly from that of second- and higher-layer islands. In particular, the edges of the Ni monolayer islands exhibit a strong tendency to run along the close-packed lattice directions, most pronounced visible in the needlelike and trough-like features, whereas higher-layer islands are more isotropically shaped. Since the compact monolayer and the higher-layer islands have the same lattice structure, this difference has to be attributed to the different substrate for the monolayer (Au) and the higher layers (Ni). Close inspection of the higher-layer islands reveals that the steps of these islands also consist of small sections that are oriented along the close-packed lattice directions. This suggests that close-packed steps are energetically favored for both types of islands, but that the formation of longer steps on higher-layer islands is kinetically hindered. The latter may be explained by a different mobility of Ni adatoms along the step edges of monolayer and higher-layer islands. Adatoms moving along the step of a monolayer island are adsorbed on the Au substrate, which provides a smooth surface free of other strongly adsorbed species, and, consequently, should have a high mobility. Hence, during Ni deposition the adatoms can be rapidly transported along the step to a more strongly binding kink site, resulting in smooth, close-packed steps. In contrast, Ni adatoms at steps of higher-layer islands are adsorbed on a Ni surface, which most likely is covered by strongly bound coadsorbates. This should lower the step-edge mobility and, consequently, the mean average length of close-packed step sections.

For the low overpotentials used in these experiments Ni monolayers and multilayers of very well-defined thickness and of low surface roughness can be formed. This requires long-range transport of Ni atoms to the edges of existing Ni adislands and, hence, a sufficiently high rate of Ni adatom diffusion across the terraces of already deposited islands. Both Ni and Au terraces provide a close-packed, (111)-oriented surface, on which the surface mobility of Ni adatoms should be high according to embedded atom method calculations of the activation energies for self-diffusion.[48] The growth mechanisms leading to the formation of a smooth Ni deposit will be discussed in detail in the following section. It is worth noting that much rougher Ni (electro-) deposits are formed on the more open Au(100) and Cu(100) surfaces.[42,43]

Monolayer and multilayer Ni films not only differ with respect to the shape of adislands, but also in the density of structural defects. For the monolayer this defect density is very high, as evidenced by the disordered arrangement of the dots of the observed moiré pattern. This can easily be rationalized by considering the nucleation and growth behavior of the Ni monolayer. The herringbone reconstructed Au surface provides a high number of heterogeneous nucleation sites (about 10^{12} cm^{-2}) on the Au terraces and (for $\eta \geqslant 100$ mV) at the Au steps for the Ni deposit, resulting in the simultaneous formation of many independent Ni islands. Due to the incommensurate structure of the Ni adlattice the lattices of neighboring islands are usually out of phase. Upon island coalescence these phase differences can either result in sharp domain boundaries within the Ni layer, localized within a few Ni lattice constants, or in a gradual deformation of the lattice over a longer range. Both cases cause a distortion of the moiré pattern and are observed experimentally in atomic- and mesoscopic-scale STM images. Apparently, the removal of these energetically unfavorable defects is kinetically hin-

dered in the Ni monolayer. However, upon growth of the second layer this kinetic barrier can apparently be partly overcome, resulting in a restructuring of both layers towards a better-ordered Ni deposit. This can be rationalized in the following way: As discussed in Sec. IV A the Ni lattice structure results from the balance between the contributions of the Ni-Ni interactions within the layer, on the one hand, and the corrugated adsorption potential of the Ni adatoms on the Au substrate on the other hand. The competition between those interactions also determines the height of the kinetic barrier, which has to be overcome to remove the phase shift between neighboring islands. Upon growth of the second layer the contribution of the Ni-Ni lateral interactions approximately doubles, resulting in a corresponding increase in the driving force of the restructuring process. The microscopic mechanisms leading to improved lattice order might involve rearrangement of first-layer Ni atoms at the domain boundaries (''intralayer'' restructuring) and/or transfer of surplus first-layer Ni atoms to the second layer and vice versa (''interlayer'' restructuring). Since the total Ni-Ni lateral interactions already double upon Ni bilayer formation, it is not surprising that the structural changes are most pronounced during the growth of the second layer. For each of the following layers the relative increase in the Ni-Ni interactions and, hence, the driving force for a further improvement of the order becomes progressively smaller.

D. Mechanisms of Ni deposition and dissolution

This section focuses on the atomic-scale processes during the deposition and dissolution of the Ni film and, in particular, on the origin of the perfect layer-by-layer growth and the faster growth rate of the first Ni layer, which differ qualitatively from the less uniformly thick and more slowly growing second and higher layers. The differences in both growth rate and growth mechanism suggest that one or more of the steps leading to Ni deposition, e.g., the adsorption of an ionic Ni species or the charge transfer reaction, is faster on Au than on the Ni surface. In this case Ni adatoms are deposited preferably on the Au surface, from where they diffuse to the edges of existing Ni monolayer islands. Thus deposition on top of the Ni layer would only start after the remaining bare Au surface area have become very small. Remarkably, under UHV conditions, where a clean metallic Ni film is formed and Ni adatoms are deposited equally on the Au and the Ni surface, the onset of second-layer growth occurs at much lower coverages (0.3 ML).[35,36] The preferred deposition on the Au surface in the electrochemical environment could be caused by the presence of growth-inhibiting coadsorbates on the Ni layer (see also Secs. IV C and IV E), which indeed has been suggested before.[5,8–10,20]

For the almost perfect layer-by-layer growth of the Ni deposit various thermodynamic and kinetic conditions have to be fulfilled. Under thermodynamic control the layer-by-layer (or Frank-van-der-Merwe) growth mode requires that the surface free energy of the admetal is equal or lower than the sum of the free surface energy of the substrate metal and the interface energy. Since the surface energy of Ni is considerably larger than that of Au,[49] this condition cannot be met for the pure metals. However, in the electrochemical environment the surface energies of one or both metals can be drastically altered by coadsorbates, thus providing the thermodynamic requirements for this growth mode. On the other hand, under kinetic control layer-by-layer growth requires that Ni adatoms, which are deposited in the next layer, are predominantly transported to the edges of existing Ni islands rather than forming next-layer island nuclei. This is fullfilled if the mobilities of Ni adatoms in the different layers are of comparable magnitude and if there is no pronounced extra barrier for adatoms to pass the edge of descending steps.[50] Electrodeposition at small deposition rates is close to equilibrium, i.e., close to thermodynamic control. Hence it is likely that the surface free energies are modified by adsorbates in the electrochemical environment. For UHV deposition, which usually proceeds far from equilibrium, the observed rougher topographies may be explained by a kinetically controlled growth as well as by the different surface free energy of the metal adlayer.

In agreement with these ideas, nucleation of second- and higher-layer Ni islands seems to occur predominantly at defects in the underlying Ni layer, as suggested by the following experimental observations: First, the Ni nuclei are not distributed uniformly over the surface, but cluster in certain areas, which partly can be identified with defect sites (e.g., underlying Au steps). The island nuclei are formed rapidly in the initial stages of the layer formation, whereas no new nuclei appear in the later stages of layer growth. Second, a distinctly higher island density is observed for the second layer, which grows on top of the highly defective Ni monolayer. Third, in contrast to the observed layer-by-layer growth higher-layer nuclei can occasionally form on top of islands with diameters of less than 50 Å, which can be only rationalized by heterogeneous nucleation at defects within these islands. Taking into account that the defect density decreases with increasing film thickness (see Sec. IV C) also the density of possible nucleation sites should decrease, which may further promote the growth of smooth films. In addition, most of the defects result from domain boundaries in between two merging islands. These boundaries are formed in the later stages of layer growth, and, hence, are not available at lower-layer occupation, preventing heterogeneous nucleation of next-layer islands in the early stages of layer occupation.

Finally, a very different mechanism is observed for the inverse process, the dissolution of the Ni films. Although Ni islands are also dissolved from the step edges, Ni is not removed in a strict layer-by-layer-like fashion. Instead, dissolution proceeds mainly via the formation of etch pits, which apparently reach down to the Au substrate. The distribution of the etch pits is not very uniform and even after prolonged etch times some areas of the Ni film are completely free of pits. This suggests that, similar as for Ni nuclei formation during deposition, etch pits nucleate preferentially at structural defects in the Ni film. The slow rate of this process even at potentials significantly more anodic than the Ni^0/Ni^{2+} Nernst potential indicates that Ni dissolution is kinetically hindered, which has been attributed to passivation by a coadsorbate.[6,9,10,20,51] Hence, for the dissolution of the topmost Ni layer the stabilizing effect of the passivating adspecies has to be overcome. In contrast, after removal of the surface Ni layer the underlying Ni is not passivated and, therefore, should be dissolved more easily (assuming that

repassivation can be neglected). This mechanism could explain why the etch pits extend over several Ni layers down to the inert Au substrate.

E. Role of the anions and nature of the coadsorbed species

The same atomic and defect structure of the Ni deposit and the same nucleation and growth behavior was observed in pure Ni sulfate, Ni nitrate, and Watts solution, demonstrating that the influence of the anion species (sulfate, nitrate, chloride, borate) on the structure and the principal deposition mechanisms is negligible. The only noticeable differences between the different electrolytes were small variations in the overpotentials and the absolute growth rates, which may indicate an influence of the anions on the charge transfer reaction (e.g., due to Ni complex formation). It is noteworthy that even in Ni nitrate solution a metallic Ni film is formed, in contrast to previous reports.[15] One may conclude that the growth of the ultrathin Ni films studied here is dominated by the interaction with the substrate rather than the electrolyte. This is supported by similar *in situ* STM studies of Ni electrodeposition on Au(100) (Ref. 43) and Cu(100),[42] where the structure and growth behavior are drastically different.

Nevertheless, the observed deposition and dissolution mechanisms and the obvious differences to the UHV-STM observations strongly indicate a coadsorbed species on top of the Ni deposit, in agreement with previous electrochemical experiments.[5,7–10,51,52] In those studies hydrogen,[8–10,51] OH^- or water,[9,52] and Ni^+ species[5,7,9] were suggested as possible adsorbates. Although the STM experiments give no direct indication on the chemical identity of the adsorbate, the observation of a metallic Ni lattice indicates that the adsorbate either forms a (1×1) adlattice, which requires a small adsorbate (H, OH^-,) or a disordered, highly mobile adlayer phase, whose molecules cannot be resolved individually by STM. At the low overpotentials used in the experiments the surface pH should not be significant increased and an OH^- adsorbate seems therefore unlikely. Most probably, the Ni surface is terminated by hydrogen, which is known to strongly chemisorb on Ni.[53]

V. CONCLUSIONS

An *in situ*, high-resolution STM study of the initial stages of Ni electrodeposition on reconstructed Au(111) electrodes at low overpotentials and in three different electrolytes as well as of the dissolution of the deposited Ni films has been presented. The data give new insight into the atomic structure and morphology of electrodeposited, ultrathin Ni films and on the corresponding nucleation and growth mechanisms. The results can be summarized as follows.

(1) Starting from the first monolayer Ni is deposited as a metallic, (111)-oriented film with well-defined orientation relative to the Au substrate.
(2) Ni is deposited in an almost perfect layer-by-layer growth up to coverages of at least 5 ML, resulting in the formation of smooth Ni films of well-defined thickness.
(3) Nucleation of Ni monolayer islands occurs at defects of the reconstructed Au(111) surface, depending on the overpotential at elbows ($\eta=80$ mV) and at Au steps ($\eta=100$ mV). Islands of the higher layers nucleate predominantly at structural defects of the underlying Ni layer.
(4) Metastable Ni islands of highly anisotropic, needlelike shape and locally well-defined orientation are formed at submonolayer coverages. These were explained by a different, anisotropic Ni lattice structure, which is pseudomorphic along the needle direction and in perpendicular direction uniaxially contracted to Ni nearest-neighbor spacings similar to those in metallic Ni.
(5) Caused by the complex nucleation and growth behavior, the Ni monolayer exhibits a high number of structural defects. Growth of the second Ni layer induces a structural rearrangement towards a less defective Ni film, reflecting the increasing importance of the lateral Ni-Ni interactions with increasing thickness of the deposit.
(6) The distinct differences in structure and growth behavior as compared to Ni films in UHV indicate the structure-decisive role of coadsorbates in the electrochemical environment. The absence of pronounced anion effects points towards adsorbed H, OH^-, or Ni^+ species.
(7) Dissolution of the Ni film proceeds via formation of etch pits. This mechanism can be attributed to passivation of the topmost Ni layer, which has to be overcome prior to etching of the underlying metallic Ni.

These results not only provide a detailed description of the initial stages of Ni deposition, but also demonstrate that atomically smooth Ni films of well-defined structure can be formed by electrodeposition. Such *in situ* grown Ni thin film electrodes may be employed in future atomic-scale studies concerning the electrochemical reactivity of Ni. Work on the electrochemical corrosion and oxidation of such Ni films is currently in progress.

ACKNOWLEDGMENTS

We gratefully acknowledge financial support by the Deutsche Forschungsgemeinschaft in the final stages of this work.

[1] F. A. Möller, O. M. Magnussen, and R. J. Behm, Phys. Rev. Lett. **77**, 5249 (1996).
[2] F. A. Möller, O. M. Magnussen, and R. J. Behm, Phys. Rev. Lett. **77**, 3165 (1996).
[3] J. Horkans, J. Electrochem. Soc. **126**, 1861 (1979).
[4] I. Epelboin, C. Gabrielli, M. Keddam, and H. Takenouti, in *Electrochemical Materials Science*, edited by J. O. Bockris, B. E. Conway, E. Yeager, and R. E. White (Plenum, New York, 1981), Vol. 4, p. 151.
[5] E. Chassaing, M. Jousselin, and R. Wiart, J. Electroanal. Chem.

157, 75 (1983).
[6] M. Fleischmann and A. Saraby-Reintjes, Electrochim. Acta **29**, 69 (1984).
[7] A. Saraby-Reintjes and M. Fleischmann, Electrochim. Acta **29**, 557 (1984).
[8] R. Wiart, Electrochim. Acta **35**, 1587 (1990).
[9] W. G. Proud and C. Müller, Electrochim. Acta **38**, 405 (1993).
[10] W. G. Proud, E. Gomez, E. Sarret, E. Vallés, and C. Müller, J. Appl. Electrochem. **25**, 770 (1995).
[11] M. Zhou, N. Myung, X. Chen, and K. Rajeshwar, J. Electroanal. Chem. **398**, 5 (1995).
[12] J. P. Hoare, J. Electrochem. Soc. **133**, 2491 (1986).
[13] K.-M. Yin and B. T. Lin, Surf. Coat. Technol. **78**, 205 (1996).
[14] J. Ji, W. C. Cooper, D. B. Dreisinger, and E. Peters, J. Appl. Electrochem. **25**, 642 (1995).
[15] C. C. Streinz, A. P. Hartman, S. Motupally, and J. W. Weidner, J. Electrochem. Soc. **142**, 1084 (1995).
[16] E. Gómez, C. Muller, W. G. Proud, and E. Vallés, J. Appl. Electrochem. **22**, 872 (1992).
[17] J. Gómez, R. Pollina, and E. Vallés, J. Electroanal. Chem. **386**, 45 (1995).
[18] Z. Chen, J. Li, and E. Wang, J. Electroanal. Chem. **373**, 83 (1994).
[19] J. Morales, S. M. Krijer, P. Esparza, S. González, L. Vásquez, R. C. Salvarezza, and A. J. Arvia, Langmuir **12**, 1068 (1996).
[20] B. E. Conway, H. Angerstein-Kozlowska, and M. A. Sattar, J. Electrochem. Soc. **130**, 1825 (1983).
[21] A. Tadjeddine, A. Lahrichi, and G. Tourillon, J. Electroanal. Chem. **360**, 261 (1993).
[22] M. Benje, M. Eiermann, U. Pittermann, and K. G. Weil, Ber. Bunsenges. Phys. Chem. **90**, 435 (1986).
[23] C. Wöll, S. Chiang, R. J. Wilson, and P. H. Lippel, Phys. Rev. B **39**, 7988 (1989).
[24] J. V. Barth, H. Brune, G. Ertl, and R. J. Behm, Phys. Rev. B **42**, 9307 (1990).
[25] D. D. Chambliss, R. J. Wilson, and S. Chiang, Phys. Rev. Lett. **66**, 1721 (1991).
[26] D. L. Abernathy, D. Gibbs, G. Grübel, K. G. Huang, S. G. J. Mochrie, A. R. Sandy, and D. M. Zehner, Surf. Sci. **283**, 260 (1993).
[27] D. M. Kolb, in *Frontiers in Electrochemistry, Vol. 2: Structure of electrified interfaced*, edited by J. Lipkowski and R. N. Ross (VCH, New York, 1993) p. 65.
[28] D. M. Kolb, Prog. Surf. Sci. **51**, 109 (1996).
[29] X. Gao, A. Hamelin, and M. J. Weaver, J. Chem. Phys. **95**, 6993 (1991).
[30] N. J. Tao and S. M. Lindsay, Surf. Sci. **274**, L546 (1992).
[31] J. Wang, A. J. Davenport, H. S. Isaacs, and B. M. Ocko, Science **255**, 1416 (1991).
[32] J. Wang, B. M. Ocko, A. J. Davenport, and H. S. Isaacs, Phys. Rev. B **46**, 10 321 (1992).
[33] O. M. Magnussen, Ph.D. thesis, University Ulm, 1993.
[34] D. M. Kolb, A. S. Dakkouri, and N. Batina, in *Nanoscale Probes of the Solid/liquid Interface*, edited by A. A. Gewirth and H. Siegenthaler (Kluwer Academic, Dordrecht, 1995), p. 263.
[35] D. D. Chambliss, S. Chiang, and R. J. Wilson, in *Structure/Property Relationships for Metal/Metal Interfaces*, edited by A. D. Romig, D. E. Fowler, and P. D. Bristowe, MRS Symposia Proceedings No. 229 (Materials Research Society, Pittsburgh, 1991), p. 15.
[36] D. D. Chambliss, R. J. Wilson, and S. Chiang, J. Vac. Sci. Technol. B **9**, 933 (1991).
[37] J. A. Meyer, I. D. Baikie, E. Kopatzki, and R. J. Behm, Surf. Sci. **365**, L647 (1996).
[38] B. Voigtländer, G. Meyer, and N. M. Amer, Phys. Rev. B **44**, 10 354 (1991).
[39] J. Wollschläger and N. M. Amer, Surf. Sci. **277**, 1 (1992).
[40] J. A. Stroscio, D. T. Pierce, R. A. Dragoset, and P. N. First, J. Vac. Sci. Technol. A **10**, 1981 (1992).
[41] O. M. Magnussen, F. A. Möller, A. Lachenwitzer, and R. J. Behm, in *Electrochemical Synthesis and Modification of Materials*, edited by P. C. Andricacos *et al.*, MRS Symposia Proceedings No. 451 (Materials Research Society, Pittsburgh, in press).
[42] A. Lachenwitzer, O. Vogt, O. M. Magnussen, and R. J. Behm, Surf. Sci. **382**, 107 (1997).
[43] F. A. Möller, Ph.D. thesis, University Ulm, 1996.
[44] J. Wiechers, T. Twomey, D. M. Kolb, and R. J. Behm, J. Electroanal. Chem. **248**, 451 (1988).
[45] K. H. Besocke, Surf. Sci. **181**, 145 (1987).
[46] S. Trasatti, in *Trends in Interfacial Electrochemistry*, edited by A. F. Silva (Reidel, Dordrecht, 1986), p. 25.
[47] M. B. Hugenschmidt, A. Hitzke, and R. J. Behm, Phys. Rev. Lett. **76**, 2535 (1996).
[48] C.-L. Liu, J. M. Cohen, J. B. Adams, and A. F. Voter, Surf. Sci. **253**, 334 (1991).
[49] H. L. Skriver and N. M. Rosengaard, Phys. Rev. B **46**, 7157 (1992).
[50] J. A. Meyer, J. Vrijmoeth, H. A. van der Vegt, E. Vlieg, and R. J. Behm, Phys. Rev. B **51**, 14 790 (1995).
[51] Y. B. Skuratnik, A. E. Kozachinskii, A. P. Pchelnikov, and V. V. Losev, J. Electroanal. Chem. **366**, 311 (1994).
[52] C. J. van der Wekken, J. Electrochem. Soc. **133**, 2293 (1986).
[53] K. Christmann, Surf. Sci. Rep. **9**, 1 (1988).